Bursty Traffic over CDMA: Predictive MAI Temporal Structure, Rate Control and Admission Control*

Junshan Zhang†, Ming Hu, and Ness B. Shroff‡

Abstract

We study data communications for the downlink in code-division-multiple-access (CDMA) networks. The focus of this paper is to exploit the predictive temporal structure of the multi-access interference (MAI) for adaptive resource allocation, particularly for rate control and admission control. We also investigate the impact of fading and traffic burstiness on the system performance. We first present our result that when the input data traffic corresponds to multiple ON-OFF heavy tailed sources, the MAI process is *asymptotically self-similar* (with Hurst parameter $1/2 < H < 1$). Thus the MAI has a nontrivial predictive temporal structure that enables accurate interference prediction. We exploit the predictive MAI structure to construct a multiple time-scale interference predictor. Rate adaptation is carried out based on the predicted interference level. Our numerical results show that this rate control scheme achieves significantly better performance than that using the packet-level MAI prediction only. We also devise a joint rate control and admission control scheme. To this end, we propose a sliding observation window scheme that has a two-tier flavor: Each observation window is divided into many time slots, rate control based on the interference prediction is conducted in each slot, and the corresponding throughput in the observation window is used for admission control accordingly.

keywords: CDMA, multi-access interference, rate control, admission control, heavy-tailed, self-similar, long-range dependent.

*Part of this paper was presented in IEEE INFOCOM 2002, New York, NY. This research is supported in part by National Science Foundation grants ANI-0208135, ANI-0207728, and an Intel Research Council grant.

†J. Zhang and M. Hu are with the Department of Electrical Engineering, Arizona State University, Tempe, AZ 85287 (e-mail: junshan.zhang@asu.edu; ming.hu@asu.edu).

‡N. Shroff is with the School of Electrical and Computer Engineering, Purdue University, West Lafayette, IN 47907 (e-mail: shroff@ecn.purdue.edu).

1 Introduction

Third generation (3G) wireless systems and beyond are expected to provide a wide variety of services ranging from low-data-rate services, such as paging to very high-data-rate services such as e-commerce, FTP, and other Internet traffic [7, 19]. The challenge of wireless networks is keeping pace with the growing level of demand. Wireless communications requires sharing a limited natural resource: the radio frequency spectrum. The data-rate capacity that a radio frequency channel can support is limited by Shannon's capacity laws [30]. Hence, in the wireless environment, one has to very carefully engineer the network such that little, if any, wireless spectrum is wasted. This requires an integrated multidisciplinary approach with expertise in wireless communications at the physical and network levels. Thus motivated, we take a data-centric viewpoint and focus on bursty data communications in code-division-multiple-access (CDMA) systems. We focus primarily on the downlink. It should be noted, however, that similar studies can also be carried out for the uplink.

CDMA systems are known to be interference-limited, and hence multi-access interference (MAI) is a key parameter that governs the system performance (see, e.g., [39, 40, 46]). In this paper, we first present a new approach to characterizing the MAI (consisting of both intercell and intracell interferences). More specifically, we incorporate explicitly both the bursty nature of data traffic and fading channel conditions, and characterize the MAI from a stochastic process perspective (in contrast to the typical perspective based on marginal distributions). This approach cuts across the physical layer, medium access control (MAC) layer and network layer, and opens a new dimension to understand the MAI temporal correlation structure. Our finding reveals that the MAI exhibits scale-invariant burstiness and is *asymptotically self-similar* across multiple time scales [47, 48] when the input traffic sources are ON-OFF heavy-tailed. The asymptotic self-similarity indicates that the MAI exhibits long-range dependent, i.e., there exists extended periods of either strong or weak interference. Clearly, the performance in any system with fixed rates may degrade significantly for a long period, either overloaded (corresponding to strong interference) or resource under-utilized (corresponding to weak interference). On the flip side, the self-similar structure of the MAI also implies that there exists a nontrivial predictive structure at coarse time scales that can be exploited for interference management resulting in improved system performance.

To exploit the predictive MAI temporal structure, we first develop a rate adaptation scheme that ameliorates the system performance. Specifically, we exploit the predictive MAI structure to construct a multiple time-scale interference predictor. Based on the predicted MAI level, our rate control can be summarized as follows: If the (predicted) future interference is weak, we increase the transmission rate via decreasing the spreading gain and/or increase the code rate; if the (predicted) future interference is strong, we decrease the transmission rate accordingly. This rate control scheme can be viewed as an example of joint adaptation across the MAC layer and the physical layer. Our results show that rate control using the multiple time-scale MAI predictor achieves significantly better performance than that with the packet-level MAI predictor only.

The predictive MAI temporal structure can also be utilized for admission control. In particular, we

devise a joint admission control and rate control scheme. Specifically, we propose a sliding observation window scheme that has a two-tier flavor: Each observation window is divided into many time slots. Rate control based on the interference prediction is conducted in each slot, and the corresponding throughput in the observation window is used for admission control. Based on the predicted (available) throughput, the system makes admission decisions, i.e., a new user is admitted if its throughput and delay requirements can be met, and vice versa if the opposite is true. Our results show that the above algorithm achieves high prediction accuracy and may be very useful for handling bursty data traffic in CDMA networks.

Our exploitation of the MAI temporal correlation structure is reminiscent of multiuser detection [39] that exploits the MAI snapshot structure at the *symbol level*—a much finer time scale, whereas rate control and admission control decisions are taken on *coarser time scales*. Clearly, resource allocation based on the predictive MAI temporal structure is a transmission technique, whereas multiuser detection is a signal processing technique implemented at the receiver end. These two methods for exploiting the MAI structure complement each other.

We also investigate the impact of fading and traffic burstiness on system performance. In a nutshell, the faster the fading, the more significant the potential gain in resource allocation (particularly rate control and admission control) via the (multiple time-scale) MAI predictor. Furthermore, the more bursty the traffic, the more gain we can expect by making use of the predictive MAI temporal structure.

In related work, there has been a great deal of research on resource allocation in CDMA networks. For example, schemes with variable spreading gains to provide multiple rates can be found in [13, 21]. Joint rate control and power control have been studied extensively (see, e.g., [14, 20, 32]). Uplink access control for CDMA systems can be found in [6, 17, 31, 45]. A call admission algorithm using the shadow cluster concept is given in [16]. Recent work [8] presents a joint admission control and flow control algorithm for wireless web browsing. Joint admission control and power control have been studied in [2, 3, 44] and the references therein. A throughput maximization scheme is provided for systems with two user classes, one consisting of data users and the other real-time users [25]. (We also note that self-similarity in network traffic has been used for congestion control in wireline networks [22, 37].)

The rest of the paper is organized as follows. The next section contains our system model. Section 3 gives our result on the MAI self-similarity and some numerical examples. We investigate in Section 4 the interference prediction for rate control and admission control. In Sections 5 and 6, we devise a rate adaptation scheme and a joint admission control and rate control algorithm. In Section 7, we examine the impact of fading and traffic burstiness. The conclusions can be found in Section 8.

2 Model Description

2.1 MAI Process in Downlink

Consider the downlink of a cellular CDMA network with many ON/OFF data users. By ON/OFF we mean that the transmission of each user is ON (active) and OFF (idle) alternatively. Based on traffic studies, we assume that the ON/OFF periods are heavy-tailed and exhibit the *Noah Effect* (i.e., have high variability or infinite variance; see [43] and the references therein). Intuitively, the Noah Effect for an individual ON/OFF source model yields ON and OFF periods that can be very large with non-negligible probability.

Let J be the number of cells under consideration. Assume that there are totally K_j ON/OFF users in cell j, $j = 1, \cdots, J$. Without loss of generality, consider user 1 in cell 1. Assume that the matched filter is employed to process the received signal. In a direct-sequence (DS) CDMA system, the interference to the desired user is the superposition of all other signals from the base stations in the network. Then, the total received power at time t due to the transmissions in cell j (in the downlink), denoted $\boldsymbol{I}_{1,j}$, is given by

$$\boldsymbol{I}_{1,j}(t) = \left(\sum_{k \in \text{cell } j} P_{k,j}(t) X_{k,j}(t) \right) g_{1,j}(t), \tag{1}$$

where $P_{k,j}(t)$ is the transmission power from the base station for user k in cell j at time t, $g_{1,j}(t)$ denotes the fading coefficient from the base station in cell j to the user under consideration, and $X_{k,j}(t) \in \{0, 1\}$ is the activity indicator for user k in cell j, i.e., $X_{k,j}(t) = 1$ if user k is ON at time t.

The MAI, consisting of both intercell interference and intracell interference, is a key parameter that limits the capacity of CDMA systems. For convenience, we use $\boldsymbol{I}(t)$ to denote the total MAI. In a large network with many users (see, e.g., [12, 18]), $\boldsymbol{I}(t)$ is well approximated by $\sum_{j=1}^{J} \boldsymbol{I}_{1,j}(t)$. (Strictly speaking, the intracell MAI is equal to $\sum_{k \neq 1, k \in \text{cell } 1} P_{k,1}(t) X_{k,1}(t) g_{1,1}(t)$. However, the signal from one single user is negligible in a large network.) Also we note that the intercell interference always exists, even though in theory the intracell interference can be eliminated by using orthogonal spreading if there is no multipath [10, 26].

The above model has a root in an earlier work [18]. A key difference between our studies is that [18] presented a snapshot analysis for power control algorithms in the uplink, whereas here we take into account the burstiness of the ON/OFF users, and characterize the MAI from a stochastic process perspective for the downlink. This new approach enables us to understand the MAI temporal correlation structure. Indeed, our results reveal the existence of a nontrivial predictive structure of the MAI process across multiple time scales, which is exploitable for efficient resource allocation [48].

2.2 Fading Channel Model

In a wireless system, fading effects can be classified as large-scale (slow) and small-scale (fast) fading effects [15, 24]. Large-scale fading includes distance-related attenuation and shadowing with duration on the order of seconds. On the other hand, fast fading is due to the scattering of the transmitted

signals off surrounding objects, and is on the order of milliseconds. Small-scale fading is superimposed on large-scale fading.

In this paper, we consider both slow and fast fading. Specifically, we assume that fading is due to distance-related attenuation, log-normal shadowing, and fast fading. The propagation attenuation is in the form of $d^{-\beta}$ where d is the distance and β is the path loss exponent, and the slow shadowing has a log-normal distribution with standard deviation $\sigma_\Omega = 8\,\text{dB}$ [33]. We use Gudmundson's auto-regressive (AR) model [11, 33] for log-normal shadowing. Suppose that the signal strength is sampled every time interval T_f, and ξ is the correlation coefficient of two consecutive samples. Then, the AR model has the form of

$$\Omega_{n+1} = \xi\Omega_n + (1-\xi)v_n, \tag{2}$$

where Ω represents the log-normal fading (in dB), v_n is zero-mean white Gaussian noise with variance $\sigma_\Omega^2(1+\xi)/(1-\xi)$, and ξ is the correlation coefficient with $0 < \xi \leq 1$. Fast Rayleigh fading (with the Doppler shift f_m [33]), is superimposed on top of slow fading. A filtered Gaussian noise model for Rayleigh fading is utilized in our study [33].

2.3 Data Traffic Model

For web traffic, it has been shown that the probability of large file size is not negligible, and that the ON duration is effectively characterized by heavy-tailed models [42]. The OFF duration is determined by the user's *thinking time*, which is also modeled as heavy-tailed [9]. Along this line, we assume throughout that the data traffic of each user is an ON/OFF process, where both ON and OFF periods are Pareto distributed (it is worth pointing out that our result on the MAI long-range dependence holds for general heavy-tailed distributions, as is clear in the proof of Theorem 3.1), that is,

$$Pr\{T > t\} = (T_{\min}/t)^\alpha, \tag{3}$$

where, $T_{\min}$ denotes the smallest possible value random variable T can take. The parameters in this traffic model are specified as follows:

a) $T_{\min,1}$: Minimal ON duration, which is determined by the minimal file size and transmission rate. According to [9] and [43], the minimal file size for web traffic is about 2 kBytes. (For example, assuming that the wireless system provides an average service of about 100 kb/s for each user, $T_{\min,1}$ is about 0.2 s for each burst transmission.)

b) $T_{\min,2}$: Minimal OFF duration, which is mainly determined by the user's think time, according to [9]. It varies from about 1 to 30 seconds.

c) α_{on}: It is determined by the slope of file size distribution, and is 1.3 in this study.

d) α_{off}: It is determined by the slope of think time distribution, and is 1.5 in this study.

For convenience, define

$$\alpha_{\min} \triangleq \min(\alpha_{\text{on}}, \alpha_{\text{off}}), \quad H_1 = \frac{3 - \alpha_{\min}}{2}.$$

For simplicity, we assume that the distributions of ON/OFF-periods are the same for all users. Our study here can be easily generalized to the cases where the distributions of ON/OFF-periods are different across users (see, e.g., [35, Theorem 2]).

3 MAI Self-Similarity and Predictive MAI Temporal Structure

3.1 Brief Overview of Self-Similar Models

In what follows, we provide a brief overview of heavy-tailed distributions and self-similar processes (see, e.g., [1, 23]).

Definition 3.1 A random variable Y has a *heavy-tailed* distribution if

$$Pr\{Y > y\} \sim \ell_1 y^{-\alpha} \tag{4}$$

as $y \to \infty$, where $0 < \alpha < 2$ and ℓ_1 is some constant. (Throughout $\ell.$ and $c.$ denote constants.)

Roughly speaking, the asymptotic shape of the distribution follows a power law, in contrast to the exponential decay. Heavy-tailed distribution, by definition, implies that a "larger" portion of the probability mass moves to the tail of the distribution, as α decreases.

Definition 3.2 For a given stationary time series $\{\boldsymbol{I}_t, t \in Z^+\}$, define the corresponding aggregated series $\boldsymbol{I}_i^{(m)}$ as

$$\boldsymbol{I}_i^{(m)} = \frac{1}{m}(\boldsymbol{I}_{im-m+1} + \ldots + \boldsymbol{I}_{im}). \tag{5}$$

Let $r(k)$ and $r^{(m)}(k)$ denote auto-correlation functions of $\{\boldsymbol{I}_t\}$ and $\{\boldsymbol{I}_i^{(m)}\}$, respectively. We say that $\{\boldsymbol{I}_t\}$ is *asymptotically (second-order) self-similar* (with Hurst parameter $1/2 < H < 1$) if the following conditions are satisfied:

$$r(k) \sim \ell_2 k^{-\beta}, \tag{6}$$

$$r^{(m)}(k) \sim r(k), \tag{7}$$

as $k \to \infty$, where $\beta = 2(1 - H)$.

A key parameter associated with self-similar processes is the above mentioned *Hurst parameter*, with range $1/2 < H < 1$. Indeed, The Hurst parameter H is sometimes called the index of self-similarity. Roughly speaking, the further H deviates from $1/2$, the more "long-range dependent" the $\{\boldsymbol{I}_t\}$ is.

3.2 MAI Self-Similarity

In the following, we characterize the MAI process in the downlink. The MAI process, $\sum_{j=1}^{J} \boldsymbol{I}_{1,j}(t)$, is a superposition of the interference processes generated by both intercell and intracell interferers. It is clear that the interference process from a user, say user k in cell j, is a product of its ON/OFF process $X_{k,j}(t)$ and the corresponding fading process $g_{1,j}(t)$. The fading coefficients can be treated as "rewards" for the underlying renewal process (i.e., the ON/OFF process). It has been showed that the superposition of many ON/OFF heavy-tailed Ethernet sources is self-similar (see, e.g., [9, 43]) where the "rewards" in each ON/OFF period are assumed as constants. Clearly, fading makes the characterization of the MAI process more challenging. Indeed, we cannot hope that the MAI process can be approximated by a Fractional Brownian Motion or even a Gaussian process [35], because the factor $g_{1,j}(t)$ in the MAI process is common for all users in cell j and there might be strong correlation between the summands of the MAI.

For technical reasons, we impose the following assumptions:

Condition 1 The sample paths of the fading process $g_{1,j}(t)$ are continuous, and the correlation function of $g_{1,j}(t)$, denoted as $\varrho_{1,j}(u)$, satisfies that $\varrho_{1,j}(u) \sim \ell_3 u^{2H_2-2}$ as $u \to \infty$, $j = 1, \ldots, J$, where $-\infty < H_2 < 1$.

Condition 2 The empirical distribution of the transmission powers of the users in cell j, converges weakly to a distribution function F_p with mean μ_p, $j = 1, \cdots, J$.

We note that the assumption on the fading process in Condition 1 is applicable to almost every practical system, and Condition 2 is a standard assumption on the transmission powers in a power-controlled network (see, e.g., [36, 46]).

We are now ready to present our result on the MAI self-similarity.

Theorem 3.1 *Suppose conditions 1–2 hold. As both W and T increase, the total accumulated MAI, $\frac{1}{T^H W^{1/2}} \int_0^{Tt} \sum_{j=1}^{J} \boldsymbol{I}_{1,j}(u)\, du$, is asymptotically (second-order) self-similar with Hurst parameter $H = \max(H_1, H_2)$.*

The proof of Theorem 3.1 has been relegated to the appendix.

3.3 Predictive MAI Temporal Structure

The MAI self-similarity, by definition, indicates that the MAI is long-range dependent and therefore there exists a MAI temporal correlation structure. Intuitively speaking, the MAI levels are highly correlated at coarser time scales. We note that the predictive MAI temporal structure exists in many realistic systems. For instance, in a cellular CDMA system, each cell has six neighboring cells, so it is likely that there are hundreds of co-channel users. Therefore, the approximation of the MAI process by long-memory models holds well. Furthermore, the predictive MAI structure exists in systems with heterogenous multimedia traffic. In what follows, we illustrate the above finding via a numerical example.

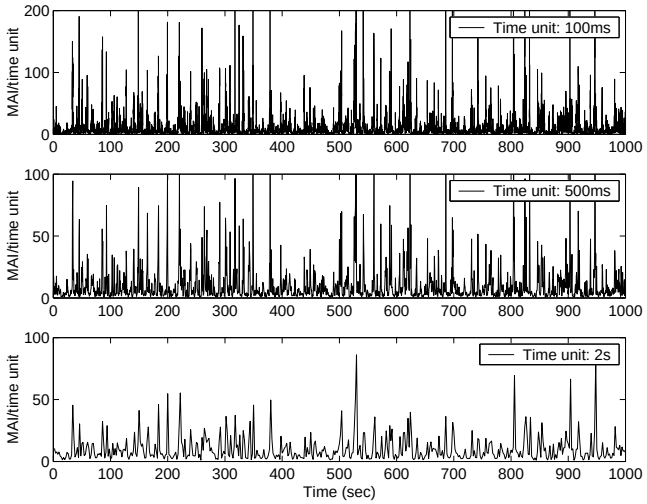

Figure 1: A pictorial "proof" of self-similar MAI: aggregated MAI exhibits "similar" burstiness on three time scales (100ms, 500ms, 2s). Some parameters of the fading channel are specified as follows: $T_f = 0.01$s, $\xi = 0.99$, $f_m = 5$Hz.

Example 1: In this example, we consider a cell with six adjacent neighboring cells. The base station in each cell uses omni-directional antennas. The total number of ON/OFF users in each cell is 120 (the average number of active (ON) users is around 15). Assume that the average transmission rate for each user is around 100 kb/s. For the MAI sequence $\{\boldsymbol{I}_n, n = 1, 2, \cdots, N\}$ in the downlink, we define the corresponding aggregated sequence at the time scale $(10m)$ ms [34]:

$$\boldsymbol{I}_i^{(m)} = \frac{1}{m}(\boldsymbol{I}_{im-m+1} + \cdots + \boldsymbol{I}_{im}), \quad i = 1, 2, \cdots, [N/m].$$

Figure 1 depicts a sequence of simple plots of the average MAI for three time units (100 ms, 500 ms, and 2 s). As is evident in Figure 1, the MAI exhibits scale-invariant burstiness at multiple time scales and "looks" self-similar at coarser time scales.

As noted before, the Hurst parameter H is sometimes called the index of self-similarity. Estimating H plays a crucial role in diagnosing self-similarity. In Figure 2, we use the variance method [42] to estimate the Hurst parameter. Specifically, we compute the sample variance at the time scale $(10m)$ ms:

$$\text{var}(\boldsymbol{I}_i^{(m)}) = \frac{1}{[N/m]} \sum_{i=1}^{[N/m]} \left(\boldsymbol{I}_i^{(m)} - \bar{\boldsymbol{I}}\right)^2, \tag{8}$$

where $\bar{\boldsymbol{I}}$ is the sample mean of the whole sequence $\{\boldsymbol{I}_n, n = 1, 2, \cdots, N\}$. The estimated Hurst parameter is 0.70, indicating that the MAI process is self-similar. (We note that the variance method is a diagnostic tool for checking if the Hurst parameter H is larger than 1/2 or not, and typically has biases [1], [4].)

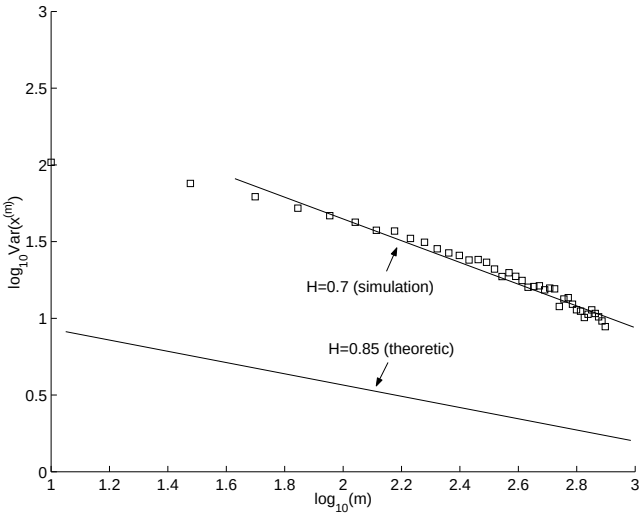

Figure 2: Estimating Hurst parameter via the variance method ($T_f = 0.01$s, $\xi = 0.99$, $f_m = 5$Hz)

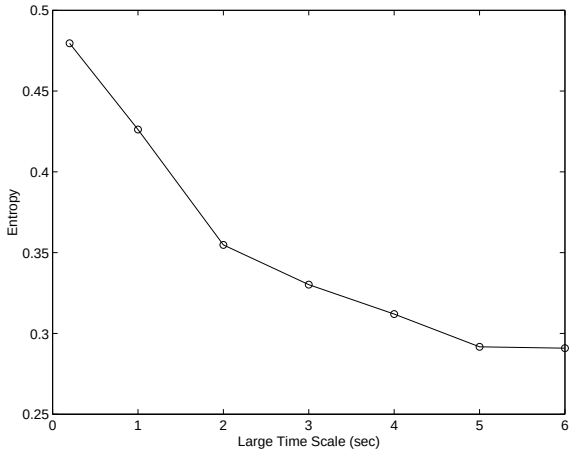

Figure 3: Entropy $\bar{S}$ versus large time scale T_m

4 Interference Prediction

Since CDMA systems are interference-limited, it is of vital importance to conduct effective interference management. To this end, a key step is to obtain accurate interference prediction, based on which we carry out resource allocation for interference management.

The MAI self-similarity ($H > 1/2$) indicates directly that there exists a predictive MAI temporal correlation structure at coarse time scales. In this section, we explore MAI prediction based on the MAI self-similarity. (We will utilize the predictive MAI temporal structure for feedback control at coarse time scales, particularly rate control and admission control in Sections 5 and 6.)

4.1 Optimum Time Scale for Exploiting Predictive MAI Temporal Structure

The time scale T_m for the MAI prediction is a critical parameter because it determines the sample size m used to predict the future interference.

There are many useful methods for determining the time scale T_m. In what follows we use two methods, namely the variance method and the entropy method, to determine T_m.

Variance method: In the following, we first use the variance method to determine T_m. Using (8), we compute the sample variance at the time scale $(10m)$ ms, and plot it against m (in the "log" scale). When the MAI is well modeled as self-similar, the plot becomes a straight line with a slope of $2H - 2$. As shown in Figure 2, the plot approaches a line as the time scale grows (beyond $\log_{10}(m) > 2$). Therefore, it is reasonable to choose $T_m = 1$s (corresponding to $\log_{10}(m) = 2$), as a large time scale for MAI prediction to utilize the MAI self-similarity.

Entropy method: Next, we use the off-line entropy method to determine T_m, along the lines of [37]. More specifically, given a time scale $T_m > 0$, we define

$$V_1 = \sum_{i \in [t-T_m, t]} \boldsymbol{I}(i), \quad V_2 = \sum_{i \in [t, t+T_m]} \boldsymbol{I}(i). \tag{9}$$

We introduce two random variables L_1, L_2 as the quantization of V_1, V_2, i.e.,

$$L_j = L_j(V_j),\ L_j \in [1, M],\ j = 1, 2, \tag{10}$$

where M denotes the number of the quantization levels. The conditional probability density is denoted as $Pr\{L_2 | L_1 = l\}$. Define

$$S_l = -\sum_{l'} Pr\{L_2 = l' | L_1 = l\} \log Pr\{L_2 = l' | L_1 = l\}. \tag{11}$$

Then the entropy is given by

$$\bar{S} = \frac{1}{M} \sum_{l=1}^{M} S_l. \tag{12}$$

Figure 3 gives the plot of $\bar{S}$ as a function of the time scale T_m, with $\alpha_{\text{on}} = 1.3$ and $\alpha_{\text{off}} = 1.5$. In Figure 3, we find that the entropy $\bar{S}$ begins to"converge" at 2 s in the sense that the entropy becomes

"flat" when the time scale is larger than 2 s, indicating that the MAI becomes more "predictable" at time scales of 2 s or larger.

Comparing the variance method and the entropy method, we notice that the estimated large time scales are on the same order. We choose $T_m = 2$ s as the large time scale for MAI prediction in the following numerical examples.

4.2 Multiple Time-Scale MAI Predictor

Since rate control in our study is implemented at the packet level (see Section 5), we devise a multiple time-scale MAI predictor which combines the MAI predictions at the packet-level and T_m. Specifically, we have that

$$\hat{\boldsymbol{I}}(i) = \lambda \hat{\boldsymbol{I}}^P(i) + (1-\lambda)\hat{\boldsymbol{I}}^L(i),\ 0 < \lambda \leq 1, \tag{13}$$

where $\hat{\boldsymbol{I}}^P(i)$ is the MAI prediction at the packet level, and $\hat{\boldsymbol{I}}^L(i)$ is the MAI prediction at T_m. We adopt a measurement-based MAI predictor at the packet level:

$$\hat{\boldsymbol{I}}^P(i) = \boldsymbol{I}_{i-1}. \tag{14}$$

In the following, we elaborate on the MAI prediction at time scale T_m. In light of the limited computing and storage capabilities at the mobile user end, we propose to use the following measurement-based MAI prediction at T_m:

$$\hat{\boldsymbol{I}}^L(i) = \frac{1}{m} \sum_{n=i-m}^{i-1} \boldsymbol{I}_n, \tag{15}$$

where $\boldsymbol{I}_n$ is the measured MAI level for the nth packet, and m is the number of samples within T_m.

5 Rate Control

In a large CDMA network with many users, the signal-to-interference-plus-noise ratio (SINR) can be well approximated as

$$\mathrm{SINR}_{1,1}(t) = \frac{P_{1,1}(t) g_{1,1}(t)}{\sigma^2 + \frac{1}{G_{1,1}(t)} \sum_{j=1}^{J} \boldsymbol{I}_{1,j}(t)}, \tag{16}$$

where $G_{1,1}(t)$ is the processing gain of the desired user in cell 1, and σ^2 is the variance of the ambient additive white Gaussian noise. Furthermore, $G_{1,1}(t) = W/R_{1,1}(t)$, where $R_{1,1}(t)$ is the transmission rate, and W is the bandwidth.

As noted before, MAI exhibits scale-invariant burstiness at multiple time scales, and the "DC" component of interference can be either strong or weak for a relatively long period. Therefore, for systems with fixed transmission rates, there exist concentrated periods where the MAI is strong or the MAI is weak. In the following, we explore rate control to improve the system performance.

5.1 Rate Adaptation Algorithm

Rate control is a central technique for interference management in bursty data systems. Next we devise an easy-to-implement rate adaptation scheme based on the multiple time-scale MAI prediction. The underlying rationale can be summarized as follows: If the (predicted) future MAI is weak, we increase the transmission rate via decreasing the spreading gain or increasing the code rate or a combination thereof; if the (predicted) future MAI is strong, we decrease the transmission rate accordingly.

We assume that a continuous transmission rate can be achieved. However, in practical systems, the spreading gain can take values 2^k (k is an integer) only. So, in order to achieve a continuous transmission rate, we need to combine spreading gain control with adaptive coding. Specifically, we decompose the bandwidth redundancy (expansion) into two parts [38]:

$$G = G_s + G_c \text{ (dB)}, \tag{17}$$

where G_s is the bandwidth redundancy corresponding to spreading, and G_c denotes the bandwidth redundancy corresponding to coding.

For adaptive coding, we can choose rate compatible punctured convolutional codes or Turbo codes (the design of coding schemes is beyond the scope of this paper). Suppose that there are N_r types of code rate modes available. We can construct a look-up table, via calculating the processing gain G for each combination of spreading gain G_s and code rate R_c. During the course of on-line control, the base station determines the pattern $\{G_s, R_c\}$ in the look-up table for certain desired SINR. Figure 4 gives a simple block diagram for the above algorithm.

Our rate control algorithm can be summarized briefly as follows:

1) The mobile user measures the strength of its downlink signal and the MAI. At the end of each packet, it makes a prediction of the MAI level for the next packet transmission, using the multiple time-scale MAI predictor.

2) The mobile user feeds the signal strength and the predicted MAI level back to the base station.

3) The base station determines the transmission rate to achieve the target SINR, and the corresponding spreading gain and code rate for the next packet transmission.

4) The base station adjusts the transmission rate accordingly.

5.2 Numerical Examples

In what follows, we evaluate the performance when the above rate control algorithm is applied to the example in Section 3. We assume that if the SINR of one entire packet is higher than the target SINR (denoted as γ), this packet is transmitted successfully, otherwise the packet is lost. The corresponding throughput is also called *goodput* [29]. Then, the average throughput is given by

$$\widetilde{\text{Th}} = \frac{1}{N} \sum_{i=1}^{N} \text{sgn}(\text{SINR} - \gamma) \cdot R_i, \tag{18}$$

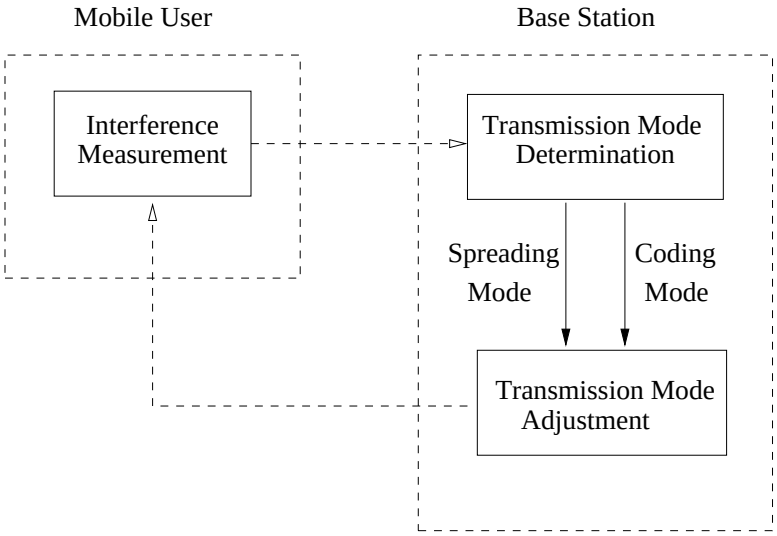

Figure 4: A simple diagram for transmission rate control

where

$$\mathrm{sgn}(z) = \begin{cases} 1 & \text{when } z > 0 \\ 0 & \text{otherwise,} \end{cases}$$

and R_i is the transmission rate of packet i.

Let $\widetilde{\mathrm{Th}}^p$ denote the average throughput of a system using the packet-level MAI predictor only and $\widetilde{\mathrm{Th}}^m$ denote the one using the multiple time-scale MAI predictor. Define the relative throughput gain δ_{Th} as

$$\delta_{\mathrm{Th}} = \frac{\widetilde{\mathrm{Th}}^m - \widetilde{\mathrm{Th}}^p}{\widetilde{\mathrm{Th}}^p}. \tag{19}$$

We now compare the performance of two schemes: Scheme 1 employs the multiple time-scale MAI predictor with $T_m = 0.2\,\mathrm{s}$, and Scheme 2 uses the multiple time-scale MAI predictor with $T_m = 2\,\mathrm{s}$. In this example, we assume that the packet duration T_p is 10 ms, the bandwidth is 10 MHz, and the target SINR threshold is 4 dB for data services. Our results are given in Figure 5. As would be expected, Scheme 2 achieves a larger throughput gain than Scheme 1. The underlying rationale is that we can get more accurate MAI prediction using the multiple time-scale method, and the choice of the large time scale also affects the prediction accuracy.

Feedback delay may exist in practical systems. It is natural to expect that feedback delay would diminish the accuracy of prediction. The effect of feedback delay on the system performance deserves consideration. In our simulation, the feedback delay is on the order of tens of milliseconds [19]. Figure 5 shows that the relative throughput gain increases with the feedback delay. Our intuition is that the larger the feedback delay is, the less accurate the packet-level MAI prediction is, and the more useful the MAI prediction at T_m is.

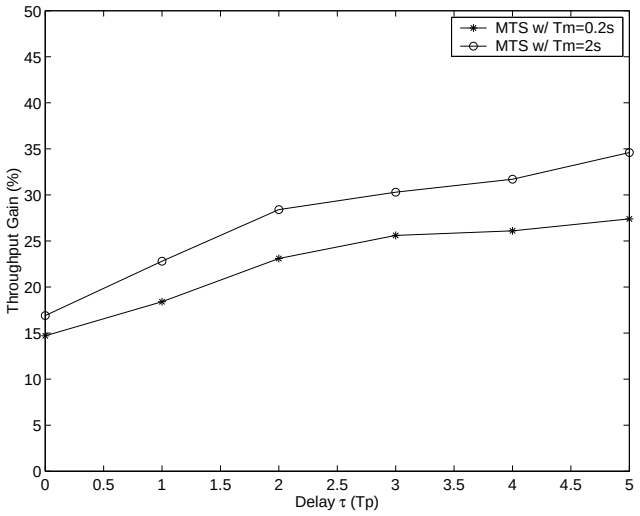

Figure 5: Throughput gain versus feedback delay ($T_f = 0.01$s, $\xi = 0.99$, $f_m = 30$Hz)

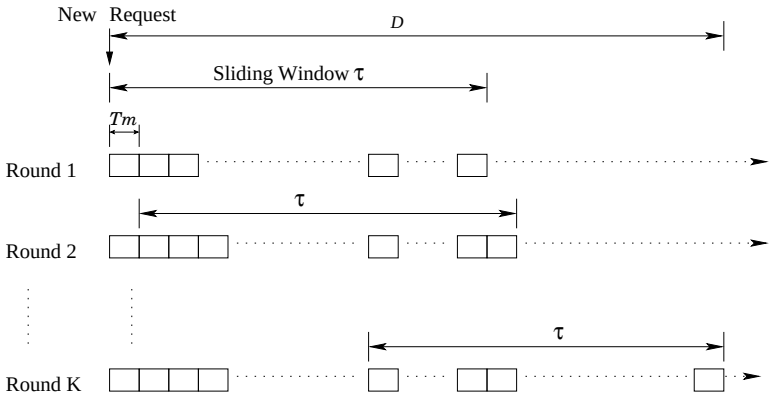

Figure 6: Admission control

6 Joint Admission Control and Rate Control

In this section, we exploit the predictive MAI structure at coarser time scales to explore admission control for data applications. For systems with voice users, admission control is based on the network capacity, which is defined as the maximum number of users that can be supported without violating their average SINR requirements [26], [29]. This approach, however, cannot be applied directly to systems with data users because of the highly bursty MAI (and hence SINR) even at large time scales. In particular, we expect that admission control schemes using the mean value of the SINR (or equivalently MAI) over one session would not work well. To resolve this issue, we propose a joint admission control and rate control scheme that has a two-tier flavor: Rate control based on the MAI prediction is conducted within a large observation window τ, and the corresponding throughput in τ is used for admission control.

Table 1: Prediction accuracy η versus α ($T_f = 0.01$s, $\xi = 0.99$, $f_m = 5$Hz)

α	1.1	1.3	1.5	1.7	1.9
Scheme A	82.7%	83.5%	86.1%	87.5%	88.3%
Scheme B	43.2%	43.7%	56.1%	59.2%	70.5%

Before we proceed to elaborate on the admission control algorithm, we need to set admission control criteria for data applications. In general, admission control involves the following two criteria [29]: 1) when a new user is admitted, the system should be able to guarantee that its QoS requirement is met; and 2) the QoS requirements of the other users already in the system should not be violated. In this study, since each user is assumed to adapt its transmission rate to the time-varying MAI, we expect that the impact of this new user on the other active transmissions is marginal. (Recall that a key feature of CDMA systems is that the performance degrades gracefully.) In light of this observation, we focus primarily on the throughput and delay requirementz of the new user. Specifically, we assume that a new user can be admitted only if its throughput requirement in a time window τ can be satisfied, that is,

$$\psi_{\text{req}} \leq \hat{\psi}_{\text{av}}, \tag{20}$$

where ψ_{req} denotes the required throughput, and $\hat{\psi}_{\text{av}}$ denotes the predicted (available) throughput within τ. We also assume that new users can tolerate delay up to some value D, and τ (less than D) is chosen according to the type of the data application.

We now present a joint admission control and rate control scheme. Specifically, a time window τ (we call it *sliding observation window*) is divided into many time slots with length T_m. The average MAI in each slot is predicted via the large time-scale MAI predictor developed in Section 4, based on which the transmission rate is adapted and the corresponding throughput within T_m is calculated. Denote $N_s = \lceil \tau / T_m \rceil$, that is, N_s denotes the number of slots in τ. The total (predicted) throughput within a sliding observation window τ is given by

$$\hat{\psi}_{\text{av}}^m = \sum_{j=1}^{N_s} \text{Th}_j, \tag{21}$$

where Th_j is the predicted throughput in slot j, $j = 1, \cdots, N_s$. We note that the rate control in the above scheme is done at the time scale T_m. We show in the following that even this simple scheme yields significant performance gain. We expect that more sophisticated rate adaptation would lead to more performance gain.

Our admission control algorithm can be summarized as follows:

1) The new user submits a connection request and also its QoS requirement in terms of $\{\psi_{\text{req}}, \tau, D\}$.

2) Based on the measurements in each T_m, the user predicts the MAI level for the next T_m, and feeds it back to the base station.

3) Based on the predicted MAI level, the base station adapts the transmission rate and updates the available throughput $\hat{\psi}_{\rm av}$ in every sliding observation window, using (21).

4) The base station makes an admission control decision using (20), that is, the user is admitted if (20) is satisfied. If not, the base station checks if the waiting time is within D, moves to the next time window if it is true, and starts Step 3 again. If the waiting time exceeds D, the request from this new user is dropped.

A simple diagram for the above scheme is shown in Figure 6.

In the following, we illustrate that the above scheme performs significantly better than the one using the mean value of the SINR (MAI) over one session. For convenience, we call the former Scheme A, and the latter Scheme B. Define the relative throughput prediction accuracy as

$$\eta = 1 - \frac{1}{N_\tau} \sum_{n=1}^{N_\tau} \frac{|\hat{\psi}_{{\rm av},n} - \psi_{{\rm av},n}|}{\psi_{{\rm av},n}}, \tag{22}$$

where $\psi_{{\rm av},n}$ is the actual available throughput in sliding window n, $\hat{\psi}_{{\rm av},n}$ is the predicted one, and N_τ is the number of sliding windows. In this example, τ is 5 minutes and T_m is 2 seconds. Table 1 gives the performance of two prediction schemes. Several observations are in order: First, the prediction accuracy of Scheme A is always better than Scheme B; second, the performance of Scheme B degrades dramatically with α, whereas Scheme A is more or less not sensitive to the degree of heavy tailedness. In a nutshell, the throughput prediction in Scheme A is significantly more accurate than that in Scheme B, and may be very useful for admission control for bursty data applications.

7 Impact of Fading and Traffic Burstiness

In the preceding sections, we have shown that the multiple time-scale MAI prediction can enhance system performance significantly. In the following, we seek to understand the following important question: How would the level of fading and traffic burstiness impact the utility of the predictive MAI temporal structure?

To start with, we examine the impact of fading on the MAI long-range dependence. In the AR model for log-normal shadowing given in (2), ξ is the correlation coefficient of the channels and T_f is the time granularity. For a fixed T_f, the smaller ξ is, the faster the fading is. In Rayleigh fading, the Doppler shift f_m governs the fading speed. Figure 7 shows that the Hurst parameter increases as the correlation coefficient ξ grows, and Figure 8 reveals that the Hurst parameter decreases as a function of f_m. Loosely speaking, the slower the fading is, the stronger the MAI long-range dependence is likely to be. Our intuition is as follows: Recall that the MAI is a superposition of many interference processes, each of which is a product of a fading process and an ON/OFF process. We would expect that both the fading process and the ON/OFF process affect the level of the MAI long-range dependence. Then it is natural to expect that in a practical (finite-size) system, the level of the long-range dependence lies in between that of the fading process and that of the ON/OFF process. Therefore, we would

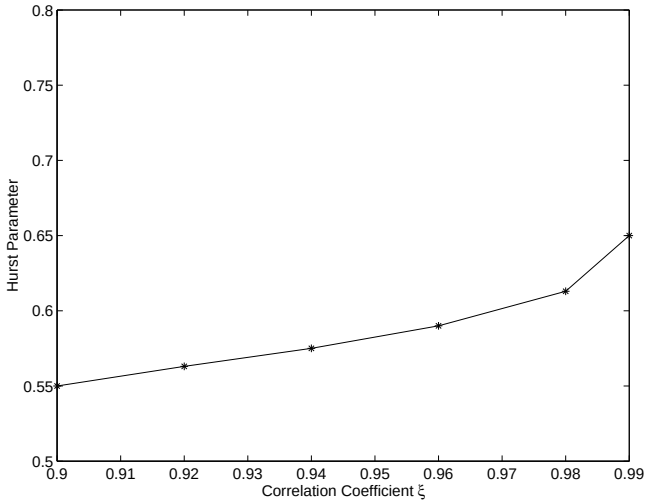

Figure 7: (Estimated) Hurst parameter versus correlation coefficient ξ ($T_f = 0.01$s, $f_m = 30$Hz)

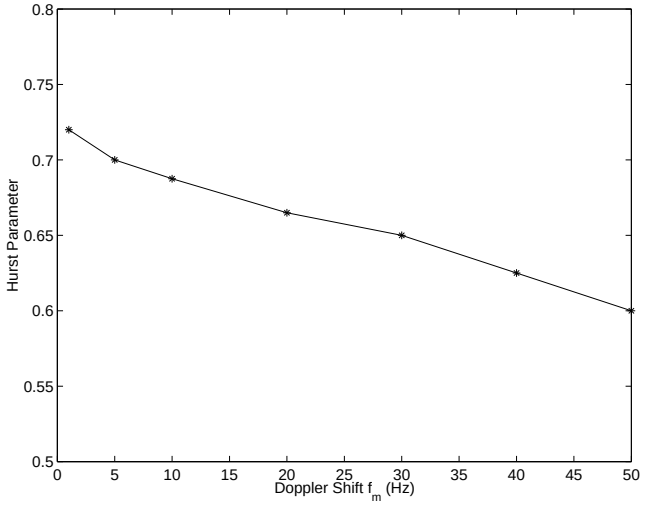

Figure 8: (Estimated) Hurst parameter versus Doppler shift f_m ($T_f = 0.01$s, $\xi = 0.99$, $f_m = 30$Hz)

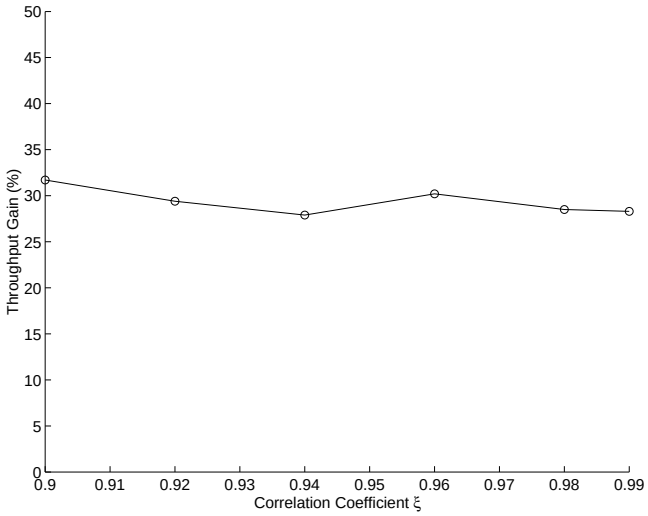

Figure 9: Rate adaptation: throughput gain versus ξ ($T_f = 0.01$s, $f_m = 30$Hz)

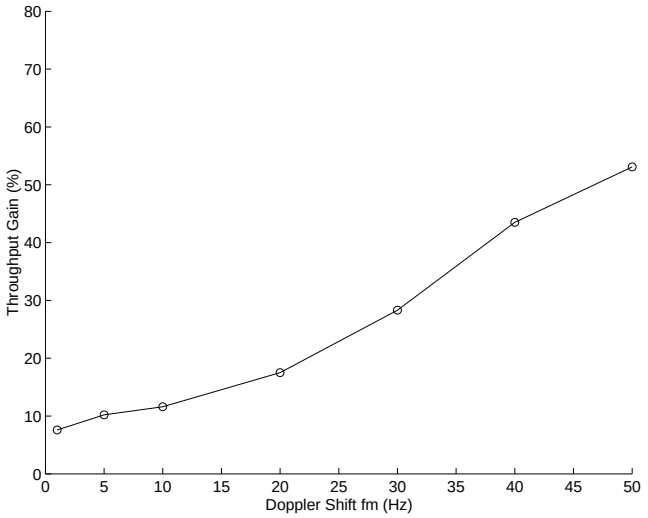

Figure 10: Rate adaptation: throughput gain versus Doppler shift f_m ($T_f = 0.01$s, $\xi = 0.99$)

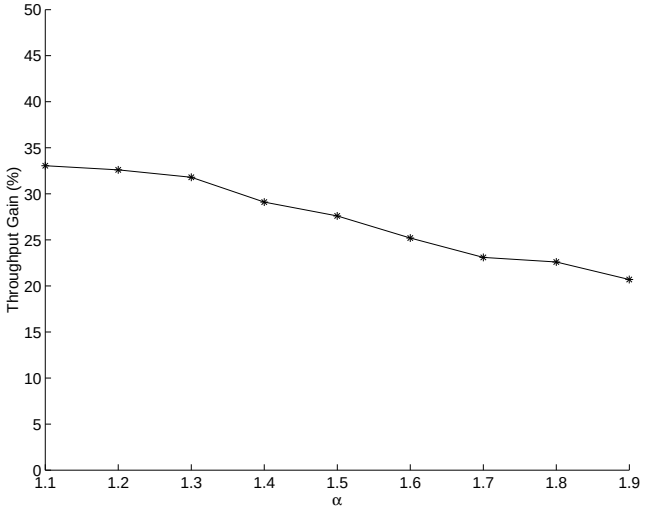

Figure 11: Rate adaptation: throughput gain versus α ($T_f = 0.01$s, $\xi = 0.99$, $f_m = 30$Hz)

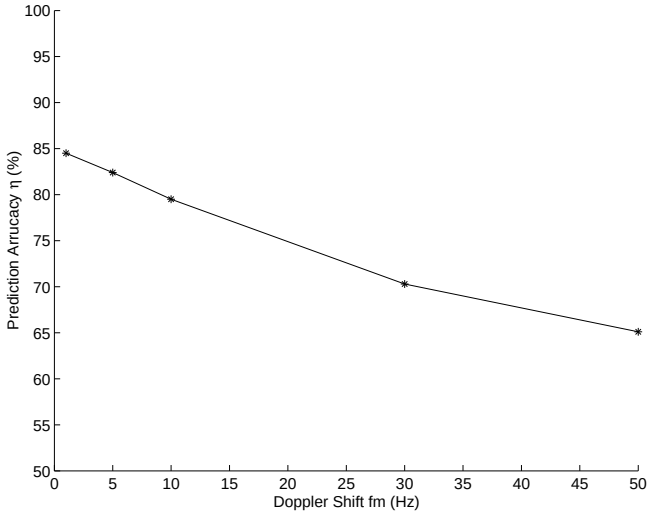

Figure 12: Admission control: prediction accuracy η versus Doppler shift f_m ($T_f = 0.01$s, $\xi = 0.99$)

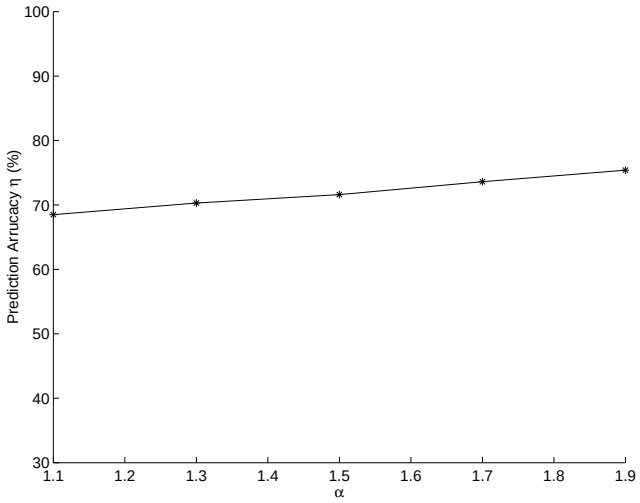

Figure 13: Admission control: prediction accuracy η versus α ($T_f = 0.01$s, $\xi = 0.99$, $f_m = 30$Hz)

expect that a slower fading results in a stronger temporal correlation. We also notice that the impact of Rayleigh fading is not as significant as the slow log-normal shadowing. This is because Rayleigh fading "modulates" the bursty traffic at smaller time scales than shadowing, and the short-range effect of Rayleigh fading can be averaged out at large time scales.

In Figures 9 and 10, we examine the impact of fading on rate adaptation. Figure 9 shows that rate adaptation is not sensitive to the correlation coefficient ξ related to log-normal shadowing. This is because the transmission rate adaptation is fast enough to trace the changing of the SINR in slowly fading channels. In Figure 10, we observe that the throughput gain increases with the Doppler shift f_m, and the rate adaptation scheme with a multiple time-scale MAI predictor can improve system performance significantly when f_m is large. The underlying rationale is as follows: When f_m increases, the accuracy of the packet-level prediction decreases. Furthermore, since the feedback delay is much smaller than T_m, its impact on the large time-scale prediction is negligible. Therefore, the rate adaption with a multiple time-scale predictor achieves significant throughput gain, when f_m becomes large.

To examine the impact of traffic burstiness, we assume for simplicity that $\alpha_{\text{on}} = \alpha_{\text{off}} = \alpha$. Figure 11 shows that the relative improvement increases when α decreases. Our intuition is that the smaller α is, the more long-range dependent the MAI would be, leading to higher prediction accuracy at the large time-scale T_m. As a result, the relative gain increases.

Next, we examine the fading effect on the joint rate adaptation and admission control scheme. Figure 12 depicts the impact of Rayleigh fading on the scheme using the multiple time-scale predictor with $T_m = 2\,\text{s}$. As would be expected, our results show that the prediction accuracy for admission control decreases as f_m grows. We also investigate the impact of traffic burstiness on the above joint rate adaptation and admission control scheme. Figure 13 shows that the smaller α is, the less the prediction accuracy becomes (but the relative gain increases).

Worth noting is that we have investigated the impact of fading and traffic burstiness on the

performance, for both systems with power control and without power control in the downlink. It turns out that the above conclusions are applicable to both cases.

8 Conclusions

In this paper, we first characterize the MAI process in CDMA networks. This approach simultaneously takes into account time-varying channel conditions and the burstiness of data traffic, and opens a new dimension to understand the corresponding MAI temporal correlation structure. Our findings show that the MAI process is asymptotically (second-order) self-similar, indicating the existence of a nontrivial predictive MAI structure at coarser time scales. This predictive MAI temporal structure is exploitable for adaptive resource allocation to achieve efficient interference management, which is the key to achieving high spectral efficiency in CDMA systems.

Next, we utilize the predictive MAI structure to explore rate control and admission control. Specifically, we propose a multiple time-scale MAI predictor for interference sensing, built on which we devise a rate adaptation scheme. The rate adaptation uses a combination of spreading gain control and adaptive coding. Our result shows that rate control using the multiple time-scale MAI predictor performs better than that using the packet-level MAI predictor only, and can improve the system throughput significantly. Furthermore, we also exploit the MAI structure to improve admission control for data applications. In particular, we introduce a sliding observation window within which rate control is conducted, and the predicted throughput in each sliding window is used for admission control. Our results reveal that this admission control scheme may be very useful for bursty data applications. We also investigate the impact of fading and traffic burstiness on the system performance. In a nutshell, the faster the fading is, the more significant gain resource allocation (particularly rate control and admission control) using the multiple time-scale MAI predictor would yield. Furthermore, the more bursty the traffic is, the more gain we can expect by making using of the predictive MAI temporal structure.

Appendix

A Proof of Theorem 3.1

Part a): Consider the MAI from cell i. For convenience, define the centered process

$$\tilde{\boldsymbol{U}}_{K_i}(t) \triangleq \frac{1}{\sqrt{K_i}} \left(\sum_{k \in C_i} P_{k,i}(t) X_{k,i}(t) - \mathbf{E} \left[\sum_{k \in C_i} P_{k,i}(t) X_{k,i}(t) \right] \right),$$

and for any $x > 0$,

$$\boldsymbol{S}_{K_i}(x) \triangleq \int_0^x g_{1,i}(t) \tilde{\boldsymbol{U}}_{K_i}(t) dt.$$

By the central limit theorem, $\tilde{\boldsymbol{U}}_{K_i}(t)$ converges weakly, as $K_i \to \infty$, to a Gaussian process with mean zero. Let $\tilde{\boldsymbol{U}}(t)$ denote the corresponding limiting Gaussian process, and define the process

$$\boldsymbol{S}(x) \triangleq \int_0^x g_{1,i}(t)\tilde{\boldsymbol{U}}(t)dt.$$

Then, the accumulated MAI from cell i over the interval $[0, x]$ is given by

$$\frac{1}{\sqrt{K_i}}\int_0^x \boldsymbol{I}_{1,i}(t)dt \;=\; \boldsymbol{S}_{K_i}(x) + \frac{1}{\sqrt{K_i}}\frac{\mu_1}{\mu_1+\mu_2}\int_0^x g_{1i}(t)\sum_{k=1}^{K_i}\mathbf{E}[P_{k,i}(t)]dt. \tag{23}$$

Using the monotone convergence theorem [28] and Condition 2, we obtain that

$$\lim_{K_i\to\infty}\frac{1}{K_i}\int_0^x g_{1i}(t)\sum_{k=1}^{K_i}\mathbf{E}[P_{k,i}(t)]dt = \mu_p\int_0^x g_{1i}(t)dt.$$

It follows from Condition 1 that

$$\text{var}\left[\int_0^x g_{1i}(t)dt\right] \sim \ell_4 x^{2H_2}, \tag{24}$$

and

$$\text{cov}\left(\boldsymbol{S}(x), \int_0^x g_{1i}(t)dt\right) = \mathbf{E}\left[\int_0^x\int_0^x g_{1,i}(u)\tilde{\boldsymbol{U}}(u)g_{1i}(v)\;du\;dv\right] = 0 \tag{25}$$

Next we show that

Step I: $\{\boldsymbol{S}_{K_i}(x), x > 0\}$ converges weakly to the process $\{\boldsymbol{S}(x), x > 0\}$.

Step II: As $x \to \infty$, $\text{var}[\boldsymbol{S}(x)] \sim \ell_5 x^{2H_1}$ if $H_2 \le H_1$ and $\text{var}[\boldsymbol{S}(x)] = o(x^{2H_2})$ if $H_2 > H_1$.

Step I: We prove, by constructing the processes on a common probability space, that $\{\boldsymbol{S}_{K_i}(x), x > 0\}$ converges weakly to the process $\{\boldsymbol{S}(x), x > 0\}$. By Condition 1, $g(t)$ is bounded for $0 < t \le x$. Since $\tilde{\boldsymbol{U}}_{K_i}(t)$ converges weakly to $\tilde{\boldsymbol{U}}(t)$, by appealing to Skorohod's Theorem [5, Theorem 25.6], there exists a probability space supporting $\tilde{\boldsymbol{U}}^*_{K_i}(t)$, $K_i = 1, 2, ...$ and $\tilde{\boldsymbol{U}}^*(t)$ jointly (where $\tilde{\boldsymbol{U}}^*_{K_i}(t) \stackrel{d}{=} \tilde{\boldsymbol{U}}_{K_i}(t)$ and $\tilde{\boldsymbol{U}}^*(t) \stackrel{d}{=} \tilde{\boldsymbol{U}}(t)$), so that $\sup_{0\le t\le 1}|\tilde{\boldsymbol{U}}^*_{K_i}(t) - \tilde{\boldsymbol{U}}^*(t)| \to 0$ as $K_i \to \infty$, almost surely. Since $g_{1,i}(t)$ is independent from the $\tilde{\boldsymbol{U}}_{K_i}(t)$'s, we can enlarge the probability space to support this $g(t)$ as well. Then, the continuity of $g_{1,i}(t)$ assures that

$$\begin{aligned} &\sup_{0\le x\le 1}\left|\int_0^x g_{1,i}(t)\tilde{\boldsymbol{U}}_{K_i}(t)dt - \int_0^x g_{1,i}(t)\tilde{\boldsymbol{U}}(t)dt\right| \\ \stackrel{d}{=} &\sup_{0\le x\le 1}\left|\int_0^x g_{1,i}(t)\tilde{\boldsymbol{U}}^*_{K_i}(t)dt - \int_0^x g_{1,i}(t)\tilde{\boldsymbol{U}}^*(t)dt\right| \to 0, \end{aligned} \tag{26}$$

as $K_i \to \infty$, which dictates directly that $\boldsymbol{S}_{K_i}(x)$ converges to $\boldsymbol{S}(x)$, for $0 < x < 1$. Now let us turn to the case when x ranges over $[0, \infty)$. Because weak convergence on $C[0, \infty)$ is, by definition, convergence with respect to the topology of uniform convergence on each finite interval (see, e.g., [41, p. 500]), i.e., a process $\{\boldsymbol{S}_{K_i}(x), x > 0\}$ converges weakly to $\{\boldsymbol{S}(x), x > 0\}$ if and only if, for each $x < \infty$, $\{\boldsymbol{S}_{K_i}(t), 0 < t \le x\}$ converges weakly to $\{\boldsymbol{S}(t), 0 < t \le x\}$. We conclude that $\{\boldsymbol{S}_{K_i}(x), x > 0\}$ converges weakly to the process $\{\boldsymbol{S}(x), x > 0\}$.

Step II: Let ζ denote that the correlation function of $\tilde{\boldsymbol{U}}$. Then,

$$\begin{aligned} \mathrm{var}[\boldsymbol{S}(x)] &= 2\ \mathrm{var}(\tilde{\boldsymbol{U}}(0))\ \mathrm{var}(g_{1,i}(0)) \int_0^x \int_0^v \zeta(u)\varrho(u)\ du\ dv \qquad (27) \\ &\quad + 2\,(\mathbf{E}[g_{1,i}(0)])^2\ \mathrm{var}(\tilde{\boldsymbol{U}}(0)) \int_0^x \int_0^v \zeta(u)\ dudv \qquad (28) \end{aligned}$$

Then, appealing to [35, Theorem 1], we have that

$$\int_0^x \int_0^v \zeta(u)\ dudv \sim c_2 x^{2H_1}. \qquad (29)$$

If $H_2 \leq H_1$, then

$$\int_0^x \int_0^v \zeta(u)\varrho(u)\ du\ dv = \int_0^x \int_0^v O(u^{4H_1-4})\ du\ dv = O(x^{2H_1}).$$

On the other hand, it is straightforward to see that when $H_1 < H_2$,

$$\int_0^x \int_0^v \zeta(u)\varrho(u)\ du\ dv = \int_0^x \int_0^v o(u^{4H_2-4})\ du\ dv = o(x^{2H_2}).$$

Hence, we have that as $x \to \infty$,

$$\begin{cases} \mathrm{var}[\boldsymbol{S}(x)] \sim \ell_5 x^{2H_1} & \text{if } H_2 \leq H_1 \\ \mathrm{var}[\boldsymbol{S}(x)] = o(x^{2H_2}) & \text{if } H_2 > H_1. \end{cases} \qquad (30)$$

Combining (23, (24), Steps I and II, we conclude that as both T and W go to infinity, the (normalized) MAI from cell i, $T^{-H}W^{-1/2}\int_0^{Tt} \boldsymbol{I}_{1,i}(u)du$ is asymptotically self-similar with the Hurst parameter $H = \max(H_1, H_2)$ (see, e.g., [27]).

Part b): A simple application of [35, Theorem 2] yields part b).

References

[1] R. J. Adler, R. E. Feldman, and M. S. Taqqu, *A Practical Guide to Heavy Tails: Statistical Techniques and Applications*. Boston: Birkhauser, 1998.

[2] M. Andersin, Z. Rosberg, and J. Zander, "Soft and safe admission control in cellular networks," *IEEE/ACM Transactions on Networking*, vol. 5, pp. 255–265, 1997.

[3] D. Ayyagari and A. Ephremides, "Power control based admission algorithms for maximing throughput in DS-CDMA networks with multimedia traffic," in *WCNC'99*, 1999.

[4] J. Beran, *Statistics for Long-Memory Processes*. Chapman & Hall/CRC, 1994.

[5] P. Billingsley, *Convergence of Probability Measures*. John Wiley & Sons, Inc., 1968.

[6] S. Choi and K. G. Shin, "An uplink CDMA system architecture with diverse QoS guarantees for heterogeneous traffic," *IEEE/ACM Transactions on Networking*, vol. 7, pp. 616–628, 1999.

[7] J. C.-I. Chuang and N. R. Sollenberger, "Spectrum resource allocation for wireless packet access with application to advanced cellular internet service," *IEEE Journal on Selected Areas in Communications*, vol. 16, pp. 820–829, 1998.

[8] C. Comaniciu, N. Mandayam, D. Famolari, and P. Agrawal, "Wireless access to the world wide web in an integrated CDMA system," preprint.

[9] M. E. Crovella and A. Bestavros, "Self-similarity in World Wide Web traffic: Evidence and possible causes," *IEEE/ACM Transactions on Networking*, vol. 5, pp. 835–846, 1997.

[10] K. S. Gilhousen, I. M. Jacobs, R. Padovani, A. J. Viterbi, L. A. Weaver Jr., and C. E. Wheatley III, "On the capacity of a cellular CDMA system," *IEEE Transactions on Vehicular Technology*, vol. 40, pp. 303–312, May 1991.

[11] M. Gudmundson, "Correlation model for shadow fading in mobile radio systems," *Electronics Letters*, vol. 27, pp. 2145–2146, 1991.

[12] S. V. Hanly, "Capacity and power control in spread spectrum macro-diversity radio networks," *IEEE Transactions on Communications*, vol. 44, no. 2, pp. 247–256, 1996.

[13] M. L. Honig and J. B. Kim, "Resource allocation for packet data transmission in DS-CDMA," in *Proc. 33th Allerton Conf.*, 1995.

[14] S. Jafar and A. Goldsmith, "Optimal rate and power adaptation for multirate CDMA," in *VTC Fall 2000*, 2000.

[15] W. C. Jakes, *Microwave Mobile Communication*. Piscataway, NJ: IEEE Press, second ed., 1994.

[16] D. Levine, I. Akyildiz, and M. Naghshineh, "A resource estimation and call admission algorithm for wireless multimedia networks using the shadow cluster concept," *IEEE/ACM Transactions on Networking*, vol. 5, pp. 1–12, 1997.

[17] T. Liu and J. Silvester, "Joint admission/congestion control for wireless CDMA systems supporting integrated services," *IEEE Journal on Selected Areas in Communications*, vol. 12, pp. 845–857, Aug. 1998.

[18] D. Mitra and J. A. Morrison, "A distributed power control algorithm for bursty transmissions on cellular, spread spectrum wireless networks," in *Proc. 5th WINLAB Workshop on Third Generation Wireless Information Networks* (J. M. Holtzman, ed.), pp. 201–212, Kluwer Academic Publishers, 1996.

[19] S. Nanda, K. Balachandran, and S. Kumar, "Adaptation techniques in wireless packet data services," *IEEE Communications Magazine*, pp. 54–64, Jan. 2000.

[20] S. Oh and K. Wasserman, "Adaptive resource allocation in power contrained CDMA mobile networks," in *WCNC'99*, 1999.

[21] S. Oh and K. Wasserman, "Dynamic spreading gain control in multi-service CDMA networks," *IEEE Journal on Selected Areas in Communications*, vol. 17, pp. 918–927, 1999.

[22] S. A. M. Ostring, H. R. Sirisena, and I. Hudson, "Rate control of elastic connections competing with long-range dependent network traffic," *IEEE Transactions on Communications*, vol. 48, pp. 1092–1111, 2001.

[23] K. Park and W. Willinger, *Self-Similar Network Traffic and Performance Evaluation.* John Wiley & Sons, Inc., 2000.

[24] R. L. Peterson, R. E. Ziemer, and D. E. Borth, *Introduction to Spread Spectrum Communications.* Prentice Hall International, Inc., 1995.

[25] S. Ramakrishna and J. M. Holtzman, "A scheme for throughput maximization in a dual-class CDMA system," *IEEE Journal on Selected Areas in Communications*, vol. 16, pp. 830–844, 1998.

[26] T. S. Rappaport, *Wireless Communications: Principles and Practice.* New Jersey: Prentice Hall, 1996.

[27] R. H. Riedi and W. Willinger, "Toward an improved understanding of network traffic dynamics," in *Self-Similar network Traffic and Performance Evaluation* (K. Park and W. Willinger, eds.), pp. 507–530, John Wiley & Sons, Inc., 2000.

[28] H. L. Royden, *Real Analysis.* Prentice Hall, Inc., third ed., 1988.

[29] A. Sampath and J. M. Holtzman, "Access control of data in integerated voice/data CDMA systems: Benifits and tradeoffs," *IEEE Journal on Selected Area in Communications*, vol. 15, pp. 1511–1526, 1997.

[30] C. E. Shannon, "A mathematical theory of communication," *Bell System Technical Journal*, vol. 27, pp. 379–423 and 623–656, July and October 1948.

[31] D. Shen and C. Ji, "Admission control of heterogeneous traffic for third generation CDMA network," in *Proceedings of IEEE INFOCOM*, (Israel), 2000.

[32] L. Song and N. Mandayam, "Hierarchical SIR and rate control on the forward link for CDMA data users under delay and error constraints," *IEEE Journal on Selected Areas in Communications*, pp. 1871–1882, Oct. 2001.

[33] G. Stuber, *Principles of Mobile Communication*. Boston, MA: Kluwer, 1996.

[34] M. S. Taqqu and V. Teverovsky, "On estimating the intensity of long-range dependence in finite and infinite variance time series," in *A practical Guide to heavy Tails: Statistical Techniques and Applications* (R. J. Adler, R. E. Feldman, and M. S. Taqqu, eds.), pp. 177–218, 1998.

[35] M. S. Taqqu, W. Willinger, and R. Sherman, "Proof of a fundamental result in self-similar traffic modeling," *Computer Communications Reviews*, vol. 27, no. 2, pp. 5–23, 1997.

[36] D. Tse and S. V. Hanly, "Linear multiuser receivers: effective interference, effective bandwidth and user capacity," *IEEE Transactions on Information Theory*, vol. 45, pp. 641–657, Mar. 1999.

[37] T. Tuan and K. Park, "Multiple time scale congestion control for self-similar network traffic," *Performance Evaluation*, vol. 36, pp. 359–386, Aug. 1999.

[38] V. V. Veeravalli, "The coding-spreading tradeoffs in cdma systems," in *Proc. 37rd Allerton Conf.*, Sept. 1999.

[39] S. Verdú, *Multiuser Detection*. Cambridge University Press, 1998.

[40] A. J. Viterbi, *CDMA—Principles of Spread Spectrum Communications*. Addison–Wesley, 1995.

[41] W. Whitt, *Stochastic-Process Limits*. New York: Springer-Verlag, 2002.

[42] W. Willinger, V. Paxson, and M. S. Taqqu, "Self-similarity and heavy tails: structural modeling of network traffic," in *A practical Guide to heavy Tails: Statistical Techniques and Applications* (R. J. Adler, R. E. Feldman, and M. S. Taqqu, eds.), pp. 27–54, Boston: Birkhauser, 1998.

[43] W. Willinger, M. S. Taqqu, R. Sherman, and D. V. Wilson, "Self-similarity through high-variability: Statistical analysis of ethernet LAN traffic at the source level," *IEEE/ACM Transactions on Networking*, vol. 5, pp. 71–86, 1997.

[44] M. Xiao, N. B. Shroff, and E. K. P. Chong, "Distributed connection admission control for power-controlled cellular wireless systems," *IEEE/ACM Transactions on Networking*, vol. 9, pp. 790–800, Dec. 2001.

[45] W. Yang and E. Geraniotis, "Admission policies for integrated voice and data traffic in CDMA packet radio networks," *IEEE Journal on Selected Areas in Communications*, vol. 12, pp. 654–664, May 1994.

[46] J. Zhang, E. K. P. Chong, and D. N. C. Tse, "Output MAI distributions of linear MMSE multiuser receivers in DS-CDMA systems," *IEEE Transactions on Information Theory*, pp. 1128–1144, Mar. 2001.

[47] J. Zhang, M. Hu, and N. B. Shroff, "Bursty data over CDMA: MAI self similarity, rate control and admission control," in *Proceedings of IEEE INFOCOM'02*, (New York, NY), pp. 391–399, 2002.

[48] J. Zhang and T. Konstantopoulos, "Self-similarity of multi-access interference processes in multimedia CDMA networks," in *Proceedings of International Symposium on Information Theory*, (Lausanne, Switzerland), p. 47, 2002.